

Article

The Crystal Structure of N α -p-tosyl-lysyl Chloromethylketone-Bound Oligopeptidase B from *Serratia Proteamaculans* Revealed a New Type of Inhibitor Binding

Vladimir I. Timofeev^{1,2,*†}, Dmitry E. Petrenko^{3,†}, Yulia K. Agapova³, Anna V. Vlaskina³, David M. Karlinsky¹, Anna G. Mikhailova¹, Inna P. Kuranova² and Tatiana V. Rakitina^{1,*} 

¹ Shemyakin-Ovchinnikov Institute of Bioorganic Chemistry, Russian Academy of Sciences, 117997 Moscow, Russia; karlinskyd@gmail.com (D.M.K.); anna.g.mikhailova@gmail.com (A.G.M.)

² Federal Scientific Research Center “Crystallography and Photonics”, Russian Academy of Sciences, 119333 Moscow, Russia; inna@crys.ras.ru

³ National Research Center “Kurchatov Institute”, 123182 Moscow, Russia; dmitry.e.petrenko@gmail.com (D.E.P.); agapova.jk@gmail.com (Y.K.A.); annavlaskina@yandex.ru (A.V.V.)

* Correspondence: tostars@mail.ru (V.I.T.); taniarakitina@yahoo.com (T.V.R.)

† V.I.T. and D.E.P.—Equivalent Participation.



Citation: Timofeev, V.I.; Petrenko, D.E.; Agapova, Y.K.; Vlaskina, A.V.; Karlinsky, D.M.; Mikhailova, A.G.; Kuranova, I.P.; Rakitina, T.V. The Crystal Structure of N α -p-tosyl-lysyl Chloromethylketone-Bound Oligopeptidase B from *Serratia Proteamaculans* Revealed a New Type of Inhibitor Binding. *Crystals* **2021**, *11*, 1438. <https://doi.org/10.3390/cryst11111438>

Academic Editor: Carlos Rodriguez-Navarro

Received: 24 October 2021

Accepted: 19 November 2021

Published: 22 November 2021

Publisher’s Note: MDPI stays neutral with regard to jurisdictional claims in published maps and institutional affiliations.



Copyright: © 2021 by the authors. Licensee MDPI, Basel, Switzerland. This article is an open access article distributed under the terms and conditions of the Creative Commons Attribution (CC BY) license (<https://creativecommons.org/licenses/by/4.0/>).

Abstract: A covalent serine protease inhibitor—Na-p-Tosyl-Lysyl Chloromethylketone (TCK) is a modified lysine residue tosylated at the N-terminus and chloromethylated at the C-terminus, one molecule of which is capable of forming two covalent bonds with both Ser and His catalytic residues, was co-crystallized with modified oligopeptidase B (OpB) from *Serratia proteamaculans* (PSPmod). The kinetics study, which preceded crystallization, shows that the stoichiometry of TCK-dependent inhibition of PSPmod was 1:2 (protein:inhibitor). The crystal structure of the PSPmod-TCK complex, solved at a resolution of 2.3 Å, confirmed a new type of inhibitor binding. Two TCK molecules were bound to one enzyme molecule: one with the catalytic Ser, the other with the catalytic His. Due to this mode of binding, the intermediate state of PSPmod and the disturbed conformation of the catalytic triad were preserved in the PSPmod-TCK complex. Nevertheless, the analysis of the amino acid surroundings of the inhibitor molecule bound to the catalytic Ser and its comparison with that of antipain-bound OpB from *Trypanosoma brucei* provided an insight in the structure of the PSPmod substrate-binding pocket. Supposedly, the new type of binding is typical for the interaction of chloromethylketone derivatives with two-domain OpBs. In the open conformational state that these enzymes are assumed in solution, the disordered configuration of the catalytic triad prevents simultaneous interaction of one inhibitor molecule with two catalytic residues.

Keywords: prolyl oligopeptidase; oligopeptidase B; crystal structure; intermediate state; serine protease; chloromethylketone inhibitors; N α -p-Tosyl-Lysyl Chloromethylketone

1. Introduction

Oligopeptidases B (OpBs, EC 3.4.21.83) are two-domain, trypsin-like serine peptidases, which belong to the S9A family of prolyl oligopeptidases (POPs) [1,2]. OpBs digest peptide bonds on the carboxyl group of the basic amino acid residues. They were found in bacteria and parasitic protozoa, considered pathogenic factors of the corresponding infections and potential pharmacological targets [3–5]. Similarly to other POP family members, OpBs consist of two domains: a catalytic α/β hydrolase domain and a propeller domain which covers the catalytic domain and restricts the size of the potential substrates to 3 kDa [6,7] (Figure 1). The active site is arranged in a cavity between the domains, which are connected by two hinge regions that provide movements of the domains relatively to each other [8].

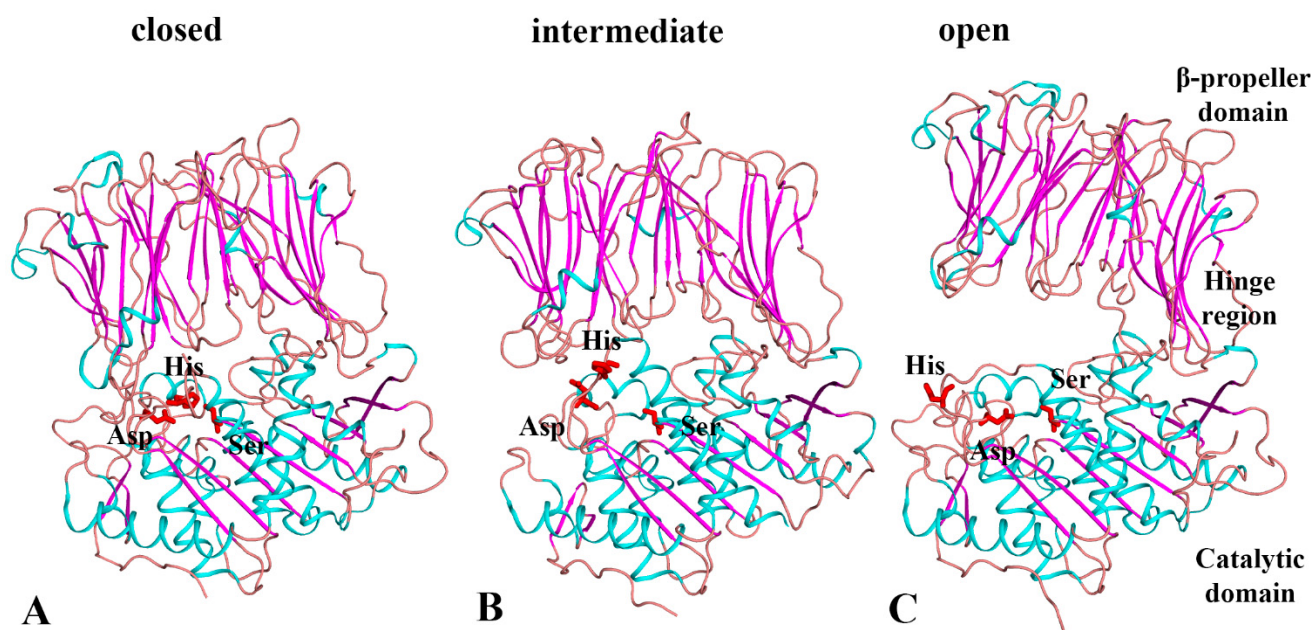


Figure 1. Domains and catalytic triad positioning in the closed, intermediate and open conformational states of OpBs. Cartoon representation of the crystal structures of AIP-bound TbOpB (PDB ID 4BP9) (A), TCK-bound PSPmod (PDB ID 7NE7) (B) and free TbOpB (PDB ID 4BP8) (C) with catalytic triad residues shown by sticks. The proteins are colored according to the secondary structure elements; the inhibitor molecules are omitted.

Structural studies of protozoan OpBs from *Leishmania major* (LmOpB) and *Trypanosoma brucei* (TbOpB) have shown that the enzymes exist in two conformational states named closed and open [9,10] (Figure 1). In the catalytically competent (closed) conformation, two domains are arranged close to each other and residues of the catalytic triad (Ser, His and Asp) are assembled in a charge relay system for the nucleophilic attack. The molecules in the catalytically incompetent (open) conformations have disordered catalytic triads, separated domains and enlarged interdomain cavities. A transition from the open to closed state includes convergence of both domains and residues of the active site with each other. During the transition, a flexible loop containing catalytic His (His-loop) changes its conformation and catalytic His swaps from the surface to the active center and occupies the position between two other components of the catalytic triad.

Recently, we have solved the 3D structures of OpB from bacteria *Serratia proteamaculans* (PSP) with the hinge region modification (PSPmod) and its derivatives PSPmodS532A and PSPE125A at 2.00, 1.88 and 2.72 Å resolutions, respectively [11]. The hinge region modification caused an inhibitory effect on the PSP catalytic activity but did not affect the basic physicochemical features of the enzyme. The structures revealed an intermediate conformational state, in which the two domains were approached to each other while the catalytic residues have not been aligned yet (Figure 1). The intermediate states were previously detected in the crystals of POPs from archaea *Pyrococcus furiosus* (PfPOP) and fungi *Galerina marginata* (GmPOP) [12,13]. In all cases, substrate-like compounds: prolylproline in the PfPOP or spermine in PSPmod, and substrate in the catalytically impaired GmPOP were presented in the interdomain cavities. According to SAXS study, both wild-type PSP and PSPmod adopted the open state in solution, while spermine caused transition to the intermediate state [11]. We suggested that the intermediate state is a naturally occurring functional state of OpBs and POPs and two-step catalytic activation, in which domain closure precedes the approachment of the catalytic triad residues, can be widely distributed in vivo. However, disordered conformation of the catalytic triad prevents the structural analysis of the catalytic and substrate-binding centers of bacterial OpBs and required additional efforts to obtain crystal structure of the enzyme in the closed state.

Structural studies of LmOpB, TbOpB and bacterial POP from *Aeromonas punctate* showed that binding of specific irreversible inhibitors, antipain (N-carboxyl-Phe-Arg-Val-Arg, AIP) and Z-Pro-Prolinal, respectively, promotes the transition of the enzymes from the open to closed conformation [9,10,14]. To initiate the transition of PSPmod to the closed state, a well-known covalent inhibitor of serine and cysteine proteases N α -p-Tosyl-Lysyl Chloromethylketone (TCK) was chosen. TCK forms a single bond with the catalytic Cys in cysteine proteases and two covalent bonds with both catalytic Ser and His residues in serine proteases [15–18]. The crystal structures of a lysine-specific endoprotease from *Lysobacter enzymogenes* (LysC) and its K30R variant in complexes with TCK represented good mimics for tetrahedral intermediates of serine proteases [16]. These crystallographically visualized intermediates provided valuable insights into the active and substrate-binding centers of the corresponding enzymes.

Analysis of the PSP and PSPmod inhibition by TCK revealed the unusual mode of inhibitor binding. The crystal structure of PSPmod bound to TCK were determined at 2.3 Å resolution and confirmed that, in contrast to previously described LysC–TCK complex, two TCK molecules were bound to one molecule of the enzyme: one to the catalytic Ser, another to the catalytic His. As a result of such mode of inhibitor binding, the intermediate state of PSPmod was preserved in the PSPmod–TCK complex and the structure did not exhibit drastic structural changes when compared with that of free PSPmod. Nevertheless, analysis of the position of Ser-bound TCK and its comparison with that of AIP in the TbOpB–AIP complex allowed us to obtain insights into the key amino acid arrangement in the substrate-binding pocket of PSPmod.

2. Materials and Methods

2.1. Production and Enzymatic Analysis of Recombinant Proteins

PSPmod-expressing plasmid was obtained as described in [11]. The expression of both recombinant proteins of wild-type PSP and PSPmod were carried out in *E. coli* BL21(DE3)RIPL (Novagen, Madison, WI, USA). Both recombinant proteins were purified to homogeneities as described in [19]. Protein sizes were controlled by electrophoresis in SDS-PAAG and protein concentrations were determined by Bradford method. Molar concentrations of the enzymes' solutions were determined using titration with p'-guanidinobenzoic acid p-nitrophenyl ester [20]; 30 kDa cutoff centrifugal filter devices (Millipore, Burlington, MA, USA) were used for buffer exchange.

Hydrolysis of N α -benzoyl-D,L-arginine-p-nitroanilide (BAPNA) (Sigma-Aldrich, St. Louis, MI, USA) was monitored as described in [21,22] by measurement of the increase in the absorption at 405 nm (0.1 M Tris-HCl, pH 8.0, 2% DMSO, 25 °C), which occurred due to the formation of free p-nitroaniline ($\Delta\epsilon_{405} = 10,400 \text{ M}^{-1} \cdot \text{cm}^{-1}$). The initial hydrolysis rate of BAPNA was determined from the initial linear part of the kinetic curve (extent of hydrolysis did not exceed 10%). Stock solution of BAPNA (20 mM) were prepared in DMSO.

2.2. Determination of Kinetic Parameters of Inhibition

Measurement of the activity of PSP and PSPmod in the course of inhibition with TCK (Sigma-Aldrich, St. Louis, MI, USA) was carried out spectrophotometrically using BAPNA (0.1 mM) as a substrate in 0.1 M Tris-HCl buffer, pH 8.0, with 50 mM CaCl₂ containing 2% DMSO (1.5 mL total volume) at 25 °C.

The kinetic parameters of the reaction between the enzyme (E) and inhibitor (I) were determined under pseudo-first order conditions ($[I] \gg [E]$) according to Kitz and Wilson [23–25].

Incubation of PSPmod (1.25 μM) or PSP (70 nM) with TCK (15–352 μM) was carried out in the reaction volume of 200–500 μL of 0.1 M Tris-HCl buffer, pH 8.0 at 25 °C. Aliquots (30–50 μL) were taken at certain time intervals and the residual activity of the enzyme was measured. At least three independent experiments for each concentration of TCK were performed.

For each concentration of the inhibitor, the apparent pseudo-first order rate constant (k') was determined from the equation:

$$\ln[E] = -k't + \ln[E_0],$$

where $[E]$ is the concentration of the active enzyme preserved during time (t) and $[E_0]$ is the initial (or total) concentration of the enzyme.

Both the classical theory of inhibition of serine proteases by one molecule of specific chloromethyl ketone [23–25], and the case when two molecules of the inhibitor binds to one molecule of the enzyme were considered (See Results and Discussion section for detailed description).

2.3. Crystallography, X-ray and Structural Analysis

PSPmod was concentrated to 20.0 mg/mL in 20 mM Tris-HCl, pH 8.0, with 100 mM NaCl; 100 mM stock solution of TCK was prepared in water. TCK was added to PSPmod in small portions with constant stirring at +4 °C until the final concentration 2.5 mM (stoichiometric ratio protein:inhibitor was about 1:10). The excess of inhibitor was removed by size-exclusion chromatography.

Crystallization of PSPmod-TCK complex were carried out in the presence of 5 mM spermine as described in [26,27]. Crystals were grown at 4 °C in 0.2 M Li₂SO₄, 0.1 M TrisHCl, pH 8.5, 30% PEG 4000. Paratone was used for cryoprotection. Diffraction data were collected at the Kurchatov synchrotron (beamline “BELOK”) as described in [26,27]. The structure was solved by the molecular replacement method using BALBES program [28]. The REFMAC5 program of the CCP4 suite [29] and the COOT interactive graphics program [30] were used for refinement and visual inspection of the electron density maps or manual rebuilding of the model, respectively. A fragment of the electron density map with TCK, Ser532 and His652 is shown in the Supplementary Figure S1.

In the structure, an asymmetric unit contained one independent copy of the protein. Visual inspection of the structure and analysis of the interdomain interface were performed using either the COOT program [30] or the PyMOL Molecular Graphics System, Version 1.9.0.0 (Schrödinger, New York, NY, USA) and the PDBEPIA [31], respectively. Superposition of the structures were carried out using the LSQKAB program [32].

Data collection and refinement statistics are presented in Table 1.

Table 1. Data collection, processing and refinement.

PDB ID Protein-Inhibitor	7NE7 PSPmod-TCK
Data collection	
Diffraction source	K4.4 beamline, NRC “Kurchatov Institute”
Wavelength (Å)	0.79272
Temperature (K)	100
Detector	CCD
Space group	P2 ₁ 2 ₁ 2 ₁
a, b, c (Å)	73.32, 101.10, 108.76
α, β, γ (°)	90.0
Unique reflections	63282
Resolution range (Å)	19.98–2.3 (2.36–2.3)
Completeness (%)	99.71 (99.01)
Average redundancy	7.92 (4614)
$\langle I/\sigma(I) \rangle$	7.98 (2.14)
R _{merge} -F* (%)	5.7 (24)
Willson B	26.2

Table 1. Cont.

PDB ID Protein-Inhibitor	7NE7 PSPmod-TCK
Refinement	
Rfact (%)	19.1
Rfree (%)	23.3
Rfree set size (%)	5
RMSD of bonds (Å)	0.008
RMSD of angles (°)	1.65
Ramachandran plot	
Most favoured (%)	99.6
Allowed (%)	0.4
No. atoms	
Protein	5545
Water	328
Ligands	124
B-factor (Å ²)	
Average	27.2
Protein	28.6
Water	26.1
Ligands	44.4

Values in parenthesis are for the highest-resolution shell. * $R_{\text{mrgd}} - F = 2 \sum_{\text{hkl}} | \langle I_1(\text{hkl}) \rangle - \langle I_2(\text{hkl}) \rangle | / \sum_{\text{hkl}} (\langle I_1(\text{hkl}) \rangle + \langle I_2(\text{hkl}) \rangle)$ [33].

2.4. Data Bank Accession Numbers

The structure of PSPmod-TCK complex has been deposited to the Protein Data Bank (PDB) under accession code (ID) 7NE7 (Table 1).

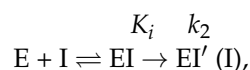
3. Results and Discussion

3.1. Inhibitory Effect of TCK on the Proteolytic Activity of PSP and PSPmod

PSPmod is OpB from *S. Proteomaculans* with hinge region modification, in which the sequence IPQQEH substituted with TEV protease recognition sequence ENLYFQ [11]. The modification inhibited enzymatic activity but promoted crystallization of the enzyme. PSPmod was crystallized in the intermediate conformational state, which represented a close-like state with a non-competent catalytic triad (see Figure 1 for illustration). Co-crystallization with the covalent inhibitor of serine proteases was a perspective approach to obtain the structure of PSPmod in the closed state. Previously, TCK, a modified lysine residue, which was tosylated at the N-terminus and chloromethylated at the C-terminus, was successfully used to obtain an insight into organization of the active and substrate-binding sites of serine and cysteine proteases [15–18].

Evaluation of the effect of TCK on the proteolytic activity of PSP and PSPmod, which preceded the crystallization experiment, showed previously not described mode of inhibitor binding.

According to the classical theory of inhibition of trypsin and other trypsin-like enzymes by TCK and other specific chloromethyl ketones [23–25], the inactivation reaction was described by the scheme (I):



where K_i is the dissociation constant and k_2 is the rate constant for the alkylation step. In this case, the apparent pseudo-first order rate constant (k') for irreversible inhibition depends on the concentration of the inhibitor according to the Michaelis–Menten Equation (1):

$$k' = k_2[I]/(K_i + [I]) \quad (1)$$

in which K_i and k_2 are obtained from a plot of the inverse of the apparent pseudo-first order rate constant (k') vs. the inverse of the concentration of the inhibitor ([I]) using Equation (2):

$$1/k' = (K_i/k_2)(1/[I]) + 1/k_2 \quad (2)$$

In the case when the enzyme binds not one, but two molecules of the inhibitor, the general scheme of the inhibition reaction for the successive binding of two molecules of the inhibitor has the form (II):



where K_i' is the dissociation constant of the complex with two inhibitor molecules. In this case, the dependence of the pseudo-first order inhibition rate constant (k') from the inhibitor concentration takes the form corresponding not to Equation (1), but to Equation (3):

$$k' = k_2[I]^2 / (K_i K_i' + K_i'[I] + [I]^2) \quad (3)$$

where the rate constant for the alkylation step (k_2) and the dissociation constant of the complex of the enzyme with one inhibitor molecule (K_i) correspond to these parameters in scheme (I); K_i' is the dissociation constant of the complex of the enzyme with two inhibitor molecules. In this case, on the graph in coordinates $1/k'$ vs. $1/[I]$, this dependence takes the form of a 2nd degree polynomial curve described by Equation (4):

$$1/k' = (K_i K_i' / k_2)(1/[I]^2) + K_i' / k_2(1/[I]) + 1/k_2 \quad (4)$$

All three kinetic parameters can be determined from the graph of the corresponding dependence.

Depending on various efficiency of binding of the first and second inhibitor molecules to the active site of the enzyme, the ratio of the equilibrium constants K_i and K_i' , as well as the concentration of the inhibitor, Equations (3) and (4) can be simplified. In particular, if the 1st inhibitor molecule binds much more efficiently than the 2nd, and the concentration of the inhibitor is high ($K_i \gg K_i'; [I] \gg K_i K_i'$), Equations (3) and (4) take the forms (5) and (6), which correspond to Equations (1) and (2), where K_i' is used instead of K_i :

$$k' = k_2[I] / (K_i' + [I]) \quad (5)$$

$$1/k' = (K_i' / k_2)(1/[I]) + 1/k_2 \quad (6)$$

The Equation (6) corresponds to a straight line in coordinates $1/k'$ vs. $1/[I]$. With a decrease of the inhibitor concentration, a deviation of the experimental curve from a straight line form a straight line should be observed.

Figure 2A,B shows that the kinetics of TCK-dependent inhibition of PSP and PSPmod catalytic activities correspond to scheme (II), and the 1st inhibitor molecule binds much more efficiently than the 2nd one. In a wide range of concentrations (21–352 μM in case of PSPmod and 15–263 μM in case of PSP), the corresponding dependences $1/k'$ vs. $1/[I]$ are described by Equation (4) (Figure 2A,B, curves 1). In the high TCK concentrations (100–352 μM in case of PSPmod and 50–263 μM in case of PSP), in accordance with the simplified Equation (6), the curves are straightened (Figure 2A,B, curves 2).

The kinetic parameters of PSP and PSPmod inhibition by TCK determined from the graphs (Figure 2A,B) are presented in Table 2. According to the Table, the first TCK molecule binds to the active site of both PSP and PSPmod much more efficiently than the second one. This difference is two orders of magnitude for the wild-type enzyme and more than an order of magnitude for PSPmod. The K_i value, which characterizes the binding efficiency of the first inhibitor molecule, for PSP, is almost an order of magnitude lower than that for PSPmod (1.8 μM vs. 11.7 μM). However, the binding efficiencies of the second TCK molecule to PSP and PSPmod are almost the same ($K_i' = 0.36$ and 0.22 mM, respectively).

The rate constant of the alkylation step (k_2) for PSP is an order of magnitude higher than for PSPmod. These data correspond to the lower hydrolytic activity of PSPmod [11].

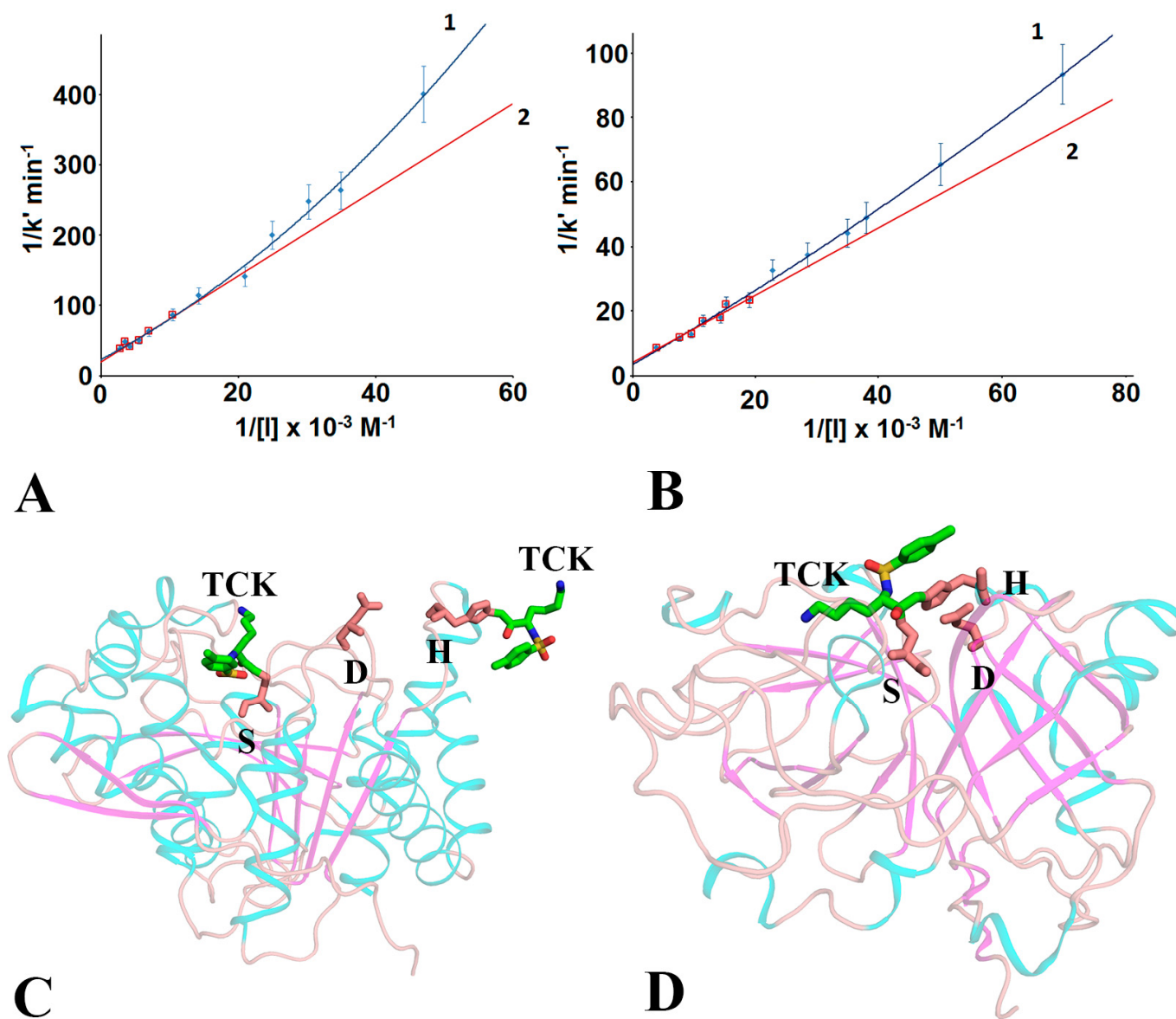


Figure 2. PSPmod binds two TCK molecules in the course of inhibition. (A) Inhibition of PSPmod (1.25 μM) by TCK in the concentration range 21–352 μM (1) and 100–352 μM (2); (B) Inhibition of PSP (70 nM) by TCK in the concentration range 15–263 μM (1) and 50–263 μM (2); (B) The data was derived from at least 3 independent experiments (A,B); (C) Two TCK molecules bound to the His and Ser catalytic residues of PSPmod (PDB ID 7NE7); (D) One TCK molecule simultaneously bound to the His and Ser catalytic residues of LysC (PDB ID 4NSY). Proteins are colored according to the secondary structure elements (C,D).

Table 2. Kinetic parameters of the PSP and PSPmod inhibition by TCK derived from 3 independent experiments (0.1 M TrisHCl, pH 8.0; substrate BAPNA; 25 $^{\circ}\text{C}$).

Enzyme Concentr.	Concentration of TCK Curve	k_2 , min^{-1}	K_i' , mM	$K_i K_i'$ $\times 10^{10}$, M^2	K_i , μM
PSPmod	21–352 μM (Figure 1A, curve 1)	0.043 ± 0.012	0.22 ± 0.05	26.2 ± 8.0	11.7 ± 4.7
1.25 μM	100–352 μM (Figure 1A, curve 2)	0.05 ± 0.01	0.31 ± 0.05	–	–
PSP	15–263 μM (Figure 1B, curve 1)	0.32 ± 0.05	0.36 ± 0.08	6.5 ± 2.3	1.8 ± 0.63
70 nM	50–263 μM (Figure 1B, curve 2)	0.27 ± 0.03	0.28 ± 0.06	–	–

For comparison, when trypsin-like enzymes bind one molecule of specific chloromethylketone, the following kinetic parameters of inhibition were obtained: $k_2 = 0.78 \text{ min}^{-1}$, $K_i = 1.2 \text{ }\mu\text{M}$ for trypsin inhibition by D-Val-Phe-Lys-CH₂C1 [24]; $k_2 = 0.78 \text{ min}^{-1}$, $K_i = 1.0 \text{ }\mu\text{M}$ for the light chain of enterokinase inhibited by Val-(Asp)₄-Lys-CH₂C1 [25].

3.2. Comparative Analysis of the Structure of PSPmod with Two Molecules of TCK Attached to the Catalytic Ser and His Residues

To visualize the molecular mechanism of the unusual mode of inhibitor binding, co-crystallization of PSPmod and TCK was performed and spatial structure of the PSPmod-TCK complex was solved at 2.3 Å resolution (Table 1). An analysis of the difference in electron density maps of PSPmod-TCK complex (PDB ID 7NE7) and free PSPmod (PDB ID 7OB1) allowed localizing two TCK molecules covalently bound to the enzyme (Figure 2C).

Previously obtained crystal structures of TCK-bound serine protease LysC (PDB ID 4NSY) showed that TCK forms covalent bonds with two residues of the catalytic triad: one bond with SerO γ (via its hemiacetal carbon atom) and another with HisN ϵ 2 (via methylene carbon) (see Figure 2D for illustration). The structure of an inhibited enzyme mimics the tetrahedral intermediate of the hydrolysis reaction [16].

The comparative analysis of the structure of TCK-bound PSPmod and those of free PSPmod (described in details in [11]) and AIP-bound LmOpB [9] (as an example of OpB in the closed conformation) is presented in Table 3. The superposition of C α -atoms of TCK-bound and ligand-free PSPmod gives RMSD 0.5 Å that indicates high similarity of the structures. According to Table 3, the ligand-bound molecule retained the intermediate conformational state established for free PSPmod in [11]. In this state, closeness of the domains is similar to that in the closed state, but the catalytic His is separated from two other catalytic residues (See Figure 1 for illustration). Such disordering of the catalytic triad is a characteristic of the open state and, normally, it associated with separation of the domains [10].

Table 3. Comparison of the crystal structures of TCK-bound PSPmod with those of ligand-free PSPmod and AIP-bound LmOpb.

PDB ID/Reference	7NE7	7OB1 [11]	2XE4 [9]
Structure name	PSPmod-TCK	PSPmod	LmOpb-AIP
Protein size/aligned area, amino acids	677/677	677/677	719/672
Conformation	interm.	interm.	closed
RMSD (C α), Å/identity, % *	0/100	0.5/100	2.2/39
Catalytic Ser—His C α -distance, Å	20.2	18.2	8.3
Catalytic SerO γ —HisN ϵ 2 distance, Å	23.0	13.9	3.1
Catalytic Asp—His C α -distance, Å	11.5	10.6	4.5
Catalytic AspO δ 2—HisN δ 1 distance, Å	10.9	9.0	2.6
The distance between centers of mass of the domains, Å	32.2	32.3	29.9
Buried surface area, cat./prop. domain, % ¹	11.6/9.9	11.3/9.4	18.3/17.3
Interface residues, cat./prop. domain, % ²	16.9/15.9	16.3/15.9	24.0/19.5
Free solvation energy of the interdomain interface (Δ^iG), kcal/M **	−12.7	−12.9	−24.0
Interdomain hydrogen bonds **	17	11	38
Interdomain salt bridges **	5	4	8

*—according to the Dali structural analysis [34]; **—according to the PDBePISA [31]; ¹—% of the buried surface area over the total surface area of the domain; ²—% of residues in the interface over the total residues in the domain.

Based on the previously published results from SAXS [11], the main confirmation of free PSP and PSPmod in solution is the open state. The transition state is insignificant in the case of PSP, which increases markedly in the case of PSPmod. In both states (open and intermediate), catalytic His652, which is located on a very mobile loop on the enzyme surface, is probably more accessible to the inhibitor than catalytic Ser532, which is located in the center of the interdomain cavity. Presumably, the interaction of TCK with His652 preceded the interaction with Ser532 and caused a local conformational rearrangement (described below), which stabilized the His652 side chain on the surface of the molecule

and prevented its movement into the interdomain cavity. Consequently, the interaction of catalytic Ser with a TCK molecule imitating the substrate did not lead to the convergence of the catalytic residues and the transition to the closed state. Spermine molecules from the crystallization solution can additionally influence the stabilization of TCK-bound PSPmod in the intermediate state.

Six spermine molecules were associated with PSPmod-TCK complex vs. five spermines found in the PSPmod structure. The spermines occupy similar positions in both structures (Figure 3A). One spermine was accommodated in the active site cavity, close to the catalytic Ser532 and two Tyr residues (Tyr452 and Tyr455), and it formed a hydrogen bond to Gln555. Another spermine molecule was located between the domains. Three spermine molecules (two in free PSPmod) were arranged close to each other inside of the interdomain cavity near surface of the propeller domain. Sixth spermine was outside of the interdomain cavity, on the surface of the propeller domain. All spermines interact with the enzyme weakly.

Further analysis of the structure showed that TCK attachment to the catalytic His652 indeed stabilized the position of His-loop: main chains and side chains of residues 647–658 became clearly visible in the electron density. His-loop with TCK-modified His652 was located on the surface of the catalytic domain and the His-bound inhibitor did not interact with any other amino acid residues (Figure 3B). At the same time, the residues 654–657 of the His-loop formed a helical coil attached to the N-terminus of the C-terminal α -helix. As a result, in TCK-bound PSPmod, the His-loop became three residues shorter and C-terminal α -helix lengthened by one coil compared to free PSPmod (Figure 3B). Thus, combination of TCK-dependent modification of the catalytic His and resulting shortness of the His-loop prevented a possibility of the His approach to other residues of the catalytic triad and the subsequent formation of an active configuration of the catalytic center.

The second TCK molecule was bound to Ser532O γ via its methylene group and it was located in the active site cavity surrounded by amino acid residues of the catalytic domain only (Figure 3C,D). Positions of the catalytic Ser532 coincided in the structures of ligand-free and TCK-bound PSPmod, whereas the C α -atoms of the catalytic Asp617 shifted by 1.69 Å. Due to opposite orientations of the Asp617 side chains, the distance between their OD1-atoms in ligand-free and TCK-bound PSPmod reached 4.9 Å. Residues, Gln619 from the catalytic domain, Arg150 and Arg151 from the propeller domain, formed the nearest surroundings of Asp617 in both structures. In ligand-free PSPmod, Asp617 was H-bound to Arg151 (Asp617O δ 1-Arg151N η 2 distance—2.75 Å). In TCK-bound PSPmod, the Asp617 side chain shifted in the direction to Arg150. As a result, the H-bond between Asp617 and Arg151 was weakened (Asp617O δ 1-Arg151N η 2 distance—3.24 Å). However, Asp617 remained H-bonded to the residue of the propeller domain. This bond restricted its movement to the Ser532 direction.

Unexpectedly, instead of the Lys side chain, which was directed to the propeller domain, the tosyl ring of TCK occupied the position of the P1 residue in the S1 sub-site of the substrate-binding pocket of PSPmod (denomination according to Schlechter and Berger nomenclature) (Figure 3D). An aromatic ring of Phe558 was located very close and nearly parallel to the tosyl ring, so a π -interaction between these two aromatic rings should favor such mode of TCK binding. Further stabilization of the TCK position was provided by side chains of Trp580, Leu572 and Tyr455 residues, which formed a large hydrophobic cluster surrounding the tosyl ring from one side. One of SO₂ oxygen of TCK was in the 2.78 Å distance from Ser532O γ , the second oxygen of SO₂ group was H-bound to Tyr455O η (2.86 Å distance) and had the S1 substrate-binding site residue (Glu576) in the nearest surrounding. Glu576 formed H-bond with Tyr455O η , which in turn was H-bound to Tyr452. Residues Ala533, Gln619 and Val620 restricted the S1 sub-site cavity from another side.

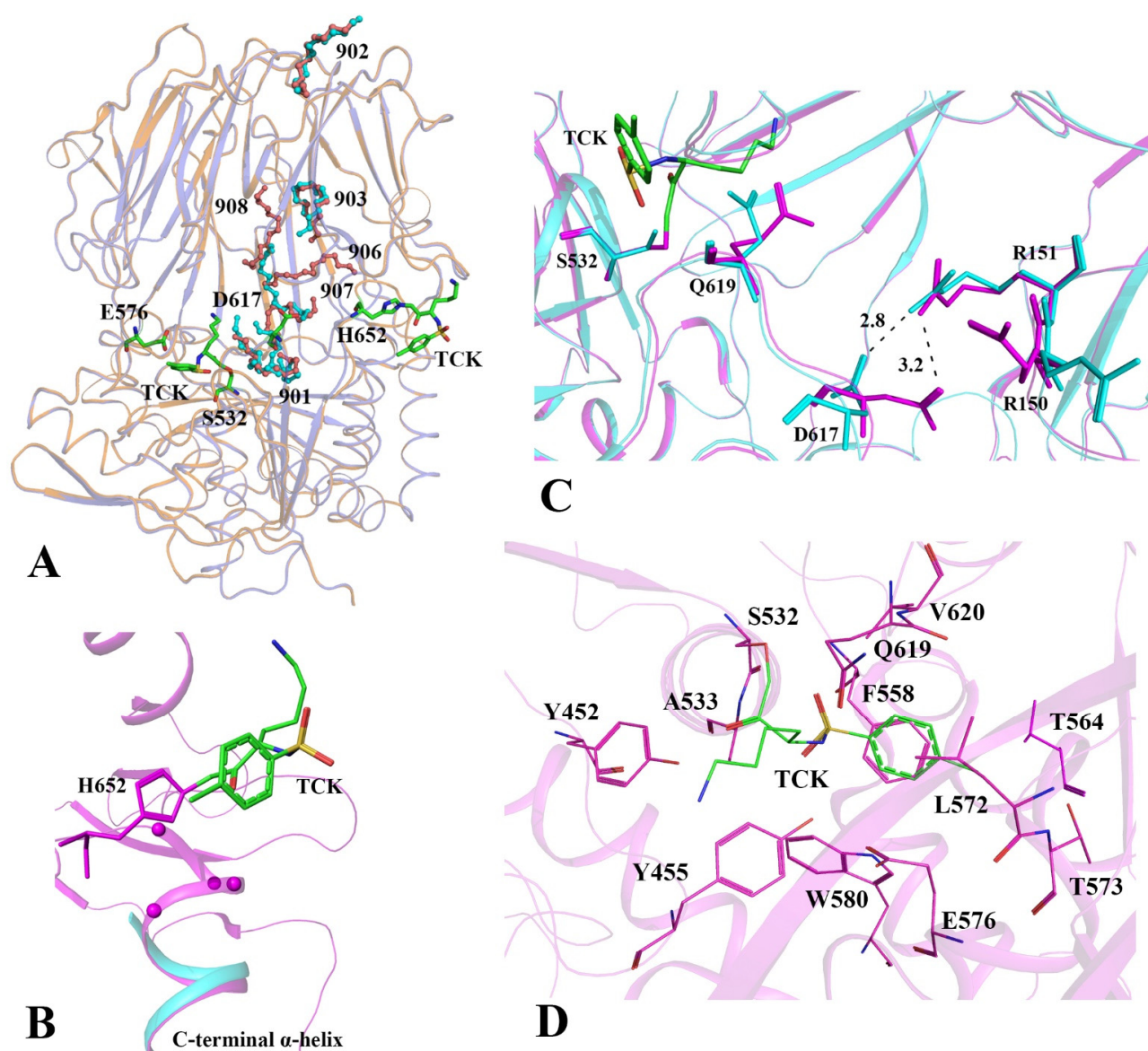


Figure 3. Structural overview of PSPmod-TCK complex and detailed views of TCK-binding sites. (A) Superposition of TCK-bound PSPmod (beige) and ligand-free PSPmod (violet). The spermine molecules in the interdomain cavities are shown in ball and sticks, colored cyan (PSPmod-TCK) or light brown (PSPmod) and numbered according to the structure of PSPmod-TCK. The catalytic triad, S1 substrate-binding center and TCK molecules are shown in green sticks in the PSPmod-TCK structure; (B) Arrangement of TCK molecule (colored green) bound to the catalytic His (colored magenta). Residues 654–657 of an additional helix coil in the N-terminus of the C-terminal α -helix in the PSPmod-TCK complex are marked in balls. A fragment of the C-terminal α -helix from ligand-free PSPmod is included for comparison and colored cyan; (C) Conformational changes in the active site area of PSPmod-TCK complex (colored magenta) compared to ligand-free PSPmod (colored cyan). TCK is colored green; (D) The amino acid surroundings of TCK (colored green) bound to the catalytic Ser and residues located in 4 Å radius from TCK are shown in magenta sticks.

LmOpB and TbOpb are the closest structural homologues of PSP (39% of identity), which were crystallized in closed conformations; the latest was found in the structures of AIP-bound enzymes [9,10]. AIP inhibits the serine proteases by formation of the covalent hemiacetal bond with catalytic SerO γ . The obtained complex mimics tetrahedral transition state in the catalytic reaction. Correspondingly, side chains of AIP residues in the P4, P3, P2 and P1 positions (according to Schleicher and Berger nomenclature) occupy substrate-binding sub-sites S4, S3, S2 and S1, respectively. The amino acids' arrangements around inhibitor molecules (TCK and AIP) covalently bound to the catalytic serines (Ser532 in

PSPmod and Ser563 in TbOpB) are shown in the superimposed structures of TCK-bound PSPmod and AIP-bound TbOpB (PDB ID 4BP9) (Figure 4). Since AIP molecule in the structure of TbOpB-AIP complex extends from the catalytic site into the interdomain cavity, and has small Val residue in the P2 position, which is not participated in intermolecular interactions, only S1 sub-site of the substrate-binding pocket of TbOpB was described in detail [10].

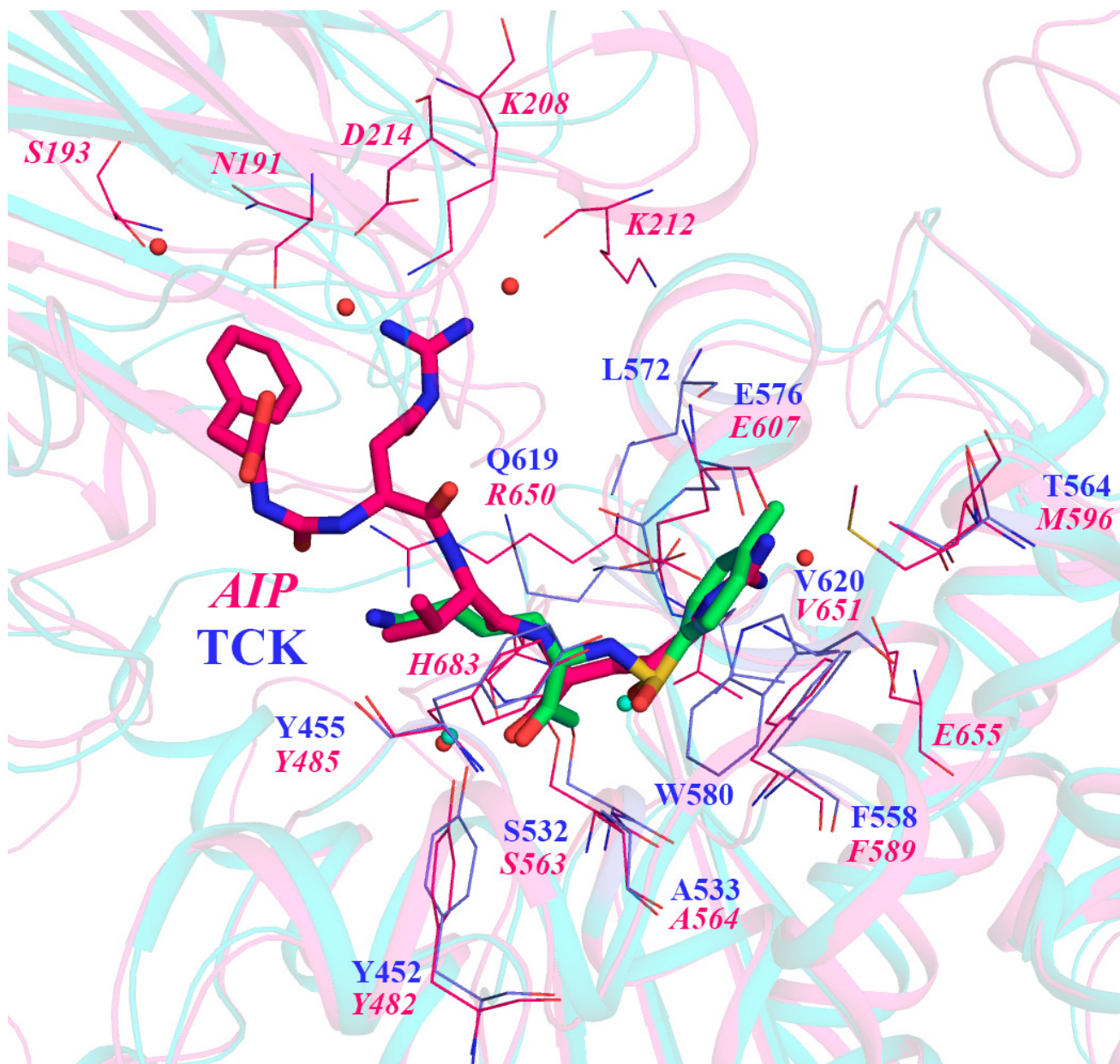


Figure 4. The superposition on α -atoms of PSPmod-TCK complex (cyan) and TbOpB-AIP complex (magenta). Amino acid residues in the nearest surrounding (4\AA) of the inhibitors bound to catalytic Ser532/563 in PSPmod-TCK/TbOpB-AIP are shown in blue and magenta sticks, respectively.

As shown in Figure 4, the tosyl ring of TCK occupied the same position as a guanidino group of P1 Arg from AIP. According to Ref. [10], the oxyanion in TbOpB-AIP is stabilized by the H-bonding to Ala564N η , which follows the catalytic Ser563. In addition, both Tyr482 and Tyr485 also participate in the oxyanion stabilization. Conserved Ala533, Tyr452 and Tyr455 from PSPmod occupy the same positions relatively to the inhibitor and can stabilize

the tetrahedral intermediate. It was proven that primary specificity of TbOpB to basic substrates (preferentially to Arg) was caused by specific interactions of the P1 residue of the substrate with Glu607; this interaction was additionally supported by π -stacking interactions between the guanidino group of P1 Arg and side chain of Phe589 [10]. In PSPmod, conserved Glu576 and Phe558 were located in similar positions near the tosyl ring of TCK.

As was mentioned above, AIP has Val residue in the P2 position, which, due to its small side chain, does not involve in any interactions. Moreover, there are not obvious acidic residues that could interact with preferential Arg in the P2 position of the substrate, but Tyr485 in TbOpB and Tyr452 in PSPmod are well positioned to interact with the P2 Arg via a π -stacking interaction (Figure 4).

Thus, despite the fact that binding of two TCK molecules to PSPmod led to an unproductive complex with disrupted catalytic triad, the superposition of TCK-bound PSPmod and AIP-bound TbOpB provided an insight in the substrate-binding area arrangement and location of the S1 and S2 sub-sites in PSPmod structure.

In conclusion, we would like to highlight that a new type of binding described here is supposed to be a typical interaction between chloromethylketone derivatives and two-domain OpBs. Separation of the domains and residues of the catalytic triad in the open conformational state that these enzymes are assumed in solution does not provide equal accessibility of both His and Ser catalytic residues to the inhibitors and prevents the simultaneous interaction of one inhibitor molecule with two catalytic residues.

Supplementary Materials: The following are available online at <https://www.mdpi.com/article/10.3390/cryst11111438/s1>, Figure S1. The density maps of the TCK molecules covalently bound to the catalytic Ser532 and His652 residues of PSPmod.

Author Contributions: Conceptualization, V.I.T. and T.V.R.; Methodology, I.P.K. and A.G.M.; Software, V.I.T. and D.E.P.; Validation, V.I.T. and D.E.P.; Formal Analysis, I.P.K.; Investigation, A.V.V., D.E.P., A.G.M. and Y.K.A.; Resources, T.V.R., A.V.V. and A.G.M.; Data Curation, D.E.P., V.I.T., A.G.M., D.M.K. and T.V.R.; Writing—Original Draft Preparation, I.P.K., A.G.M. and T.V.R.; Writing—Review and Editing, D.M.K. and T.V.R.; Visualization, V.I.T. and D.E.P.; Supervision, T.V.R.; Project Administration, T.V.R.; Funding Acquisition, T.V.R. All authors have read and agreed to the published version of the manuscript.

Funding: The research was funded by the Russian Science Foundation, grant number 21-74-20154, in the part of structural analysis and enzymatic kinetics. Chloromethylketone derivatives-related study was partially covered by Project #3009011, “The importance of neutrophil-derived enzymes for the processing of auto-antigens and inflammatory mediators” by Volkswagen-Stiftung. The work was also partially supported by the Ministry of Science and Higher Education within the State assignment FSRC “Crystallography and Photonics” RAS to I.P.K. (in the part of formal analysis).

Institutional Review Board Statement: Not applicable.

Informed Consent Statement: Not applicable.

Data Availability Statement: The atomic coordinates of and structural statistics of PSPmod-TCK complex has been deposited to the Protein Data Bank (PDB) under accession code (ID) 7NE7.

Acknowledgments: We acknowledge the Center for collective use “Bioorganika” of Shemyakin-Ovchinnikov Institute of Bioorganic Chemistry RAS for usage of the computing resources; Nikolaeva A. Yu. and Resource Center for Molecular and Cellular Biology of NRC “Kurchatov Institute” as well as Kurchatov specialized synchrotron radiation source (“KISI-Kurchatov”) and, particularly Dorovatovskii P.V., Lazarenko V.A., for technical support.

Conflicts of Interest: The authors declare no conflict of interest.

References

1. Polgár, L. The prolyl oligopeptidase family. *Cell. Mol. Life Sci.* **2002**, *59*, 349–362. [[CrossRef](#)] [[PubMed](#)]
2. Rawlings, N.D.; Barrett, A.J.; Thomas, P.; Huang, X.; Bateman, A.; Finn, R.D. The MEROPS database of proteolytic enzymes, their substrates and inhibitors in 2017 and a comparison with peptidases in the PANTHER database. *Nucleic Acids Res.* **2018**, *46*, D624–D632. [[CrossRef](#)] [[PubMed](#)]
3. Motta, F.N.; Azevedo, C.D.S.; Neves, B.P.; de Araújo, C.N.; Grellier, P.; de Santana, J.M.; Bastos, I.M.D. Oligopeptidase B, a missing enzyme in mammals and a potential drug target for trypanosomatid diseases. *Biochimie* **2019**, *167*, 207–216. [[CrossRef](#)] [[PubMed](#)]
4. Coetzer, T.H.; Goldring, J.P.D.; Huson, L.E. Oligopeptidase B: A processing peptidase involved in pathogenesis. *Biochimie* **2008**, *90*, 336–344. [[CrossRef](#)]
5. Mattiuzzo, M.; De Gobba, C.; Runti, G.; Mardirossian, M.; Bandiera, A.; Gennaro, R.; Scocchi, M. Proteolytic Activity of Escherichia coli Oligopeptidase B Against Proline-Rich Antimicrobial Peptides. *J. Microbiol. Biotechnol.* **2014**, *24*, 160–167. [[CrossRef](#)]
6. Fülöp, V.; Böcskei, Z.; Polgár, L. Prolyl Oligopeptidase: An Unusual β -Propeller Domain Regulates Proteolysis. *Cell* **1998**, *94*, 161–170. [[CrossRef](#)]
7. Rea, D.; Fülöp, V. Structure-Function Properties of Prolyl Oligopeptidase Family Enzymes. *Cell Biophys.* **2006**, *44*, 349–365. [[CrossRef](#)]
8. Shan, L.; Mathews, I.I.; Khosla, C. Structural and mechanistic analysis of two prolyl endopeptidases: Role of interdomain dynamics in catalysis and specificity. *Proc. Natl. Acad. Sci. USA* **2005**, *102*, 3599–3604. [[CrossRef](#)]
9. McLuskey, K.; Paterson, N.; Bland, N.D.; Isaacs, N.W.; Mottram, J. Crystal Structure of Leishmania major Oligopeptidase B Gives Insight into the Enzymatic Properties of a Trypanosomatid Virulence Factor. *J. Biol. Chem.* **2010**, *285*, 39249–39259. [[CrossRef](#)]
10. Canning, P.; Rea, D.; Morty, R.E.; Fülöp, V. Crystal Structures of Trypanosoma brucei Oligopeptidase B Broaden the Paradigm of Catalytic Regulation in Prolyl Oligopeptidase Family Enzymes. *PLoS ONE* **2013**, *8*, e79349. [[CrossRef](#)]
11. Petrenko, D.E.; Timofeev, V.I.; Britikov, V.V.; Britikova, E.V.; Kleymenov, S.Y.; Vlaskina, A.V.; Kuranova, I.P.; Mikhailova, A.G.; Rakitina, T.V. First Crystal Structure of Bacterial Oligopeptidase B in an Intermediate State: The Roles of the Hinge Region Modification and Spermine. *Biology* **2021**, *10*, 1021. [[CrossRef](#)] [[PubMed](#)]
12. Czekster, C.M.; Ludewig, H.; McMahon, S.A.; Naismith, J.H. Characterization of a dual function macrocyclase enables design and use of efficient macrocyclization substrates. *Nat. Commun.* **2017**, *8*, 1045. [[CrossRef](#)] [[PubMed](#)]
13. Ellis-Guardiola, K.; Rui, H.; Beckner, R.; Srivastava, P.; Sukumar, N.; Roux, B.; Lewis, J.C. Crystal Structure and Conformational Dynamics of Pyrococcus furiosus Prolyl Oligopeptidase. *Biochimie* **2019**, *58*, 1616–1626. [[CrossRef](#)] [[PubMed](#)]
14. Li, M.; Chen, C.; Davies, D.R.; Chiu, T.K. Induced-fit Mechanism for Prolyl Endopeptidase. *J. Biol. Chem.* **2010**, *285*, 21487–21495. [[CrossRef](#)]
15. Frydrych, I.; Mlejnek, P. Serine protease inhibitors N- α -Tosyl-L-Lysinyl-Chloromethylketone (TLCK) and N-Tosyl-L-Phenylalaninyl-Chloromethylketone (TPCK) are potent inhibitors of activated caspase proteases. *J. Cell. Biochem.* **2008**, *103*, 1646–1656. [[CrossRef](#)]
16. Asztalos, P.; Müller, A.; Hölke, W.; Sobek, H.; Rudolph, M.G. Atomic resolution structure of a lysine-specific endoproteinase from Lysobacter enzymogenes suggests a hydroxyl group bound to the oxyanion hole. *Acta Crystallogr. Sect. D Biol. Crystallogr.* **2014**, *70*, 1832–1843. [[CrossRef](#)]
17. Drenth, J.; Kalk, K.H.; Swen, H.M. Binding of chloromethyl ketone substrate analogs to crystalline papain. *Biochemistry* **1976**, *15*, 3731–3738. [[CrossRef](#)]
18. Azarkan, M.; Maquoi, E.; Delbrassine, F.; Herman, R.; M'Rabet, N.; Esposito, R.C.; Charlier, P.; Kerff, F. Structures of the free and inhibitors-bound forms of bromelain and ananain from Ananas comosus stem and in vitro study of their cytotoxicity. *Sci. Rep.* **2020**, *10*, 19570. [[CrossRef](#)]
19. Mikhailova, A.G.; Khairullin, R.F.; Demidyuk, I.V.; Kostrov, S.V.; Grinberg, N.V.; Burova, T.V.; Grinberg, V.Y.; Rumsh, L.D. Cloning, sequencing, expression, and characterization of thermostability of oligopeptidase B from Serratia proteamaculans, a novel psychrophilic protease. *Protein Expr. Purif.* **2014**, *93*, 63–76. [[CrossRef](#)]
20. Walsh, K.; Wilcox, P. Serine proteases. *Methods Enzymol.* **2011**, *19*, 31–41. [[CrossRef](#)]
21. Mikhailova, A.G.; Rakitina, T.V.; Timofeev, V.I.; Karlinsky, D.M.; Korzhenevskiy, D.A.; Agapova, Y.K.; Vlaskina, A.V.; Ovchinnikova, M.V.; Gorlenko, V.A.; Rumsh, L.D. Activity modulation of the oligopeptidase B from Serratia proteamaculans by site-directed mutagenesis of amino acid residues surrounding catalytic triad histidine. *Biochimie* **2017**, *139*, 125–136. [[CrossRef](#)]
22. Petrenko, D.E.; Mikhailova, A.G.; Timofeev, V.I.; Agapova, Y.K.; Karlinsky, D.M.; Komolov, A.S.; Korzhenevskiy, D.A.; Vlaskina, A.V.; Rumsh, L.D.; Rakitina, T.V. Molecular dynamics complemented by site-directed mutagenesis reveals significant difference between the interdomain salt bridge networks stabilizing oligopeptidases B from bacteria and protozoa in their active conformations. *J. Biomol. Struct. Dyn.* **2019**, *38*, 4868–4882. [[CrossRef](#)] [[PubMed](#)]
23. Kitz, R.; Wilson, I.B. Esters of methanesulfonic acid as irreversible inhibitors of acetylcholinesterase. *J. Biol. Chem.* **1962**, *237*, 3245–3249. [[CrossRef](#)]
24. Collen, D.; Lijnen, H.; De Cock, F.; Durieux, J.; Loffet, A. Kinetic properties of tripeptide lysyl chloromethyl ketone and lysyl p-nitroanilide derivatives towards trypsin-like serine proteinases. *Biochim. Biophys. Acta (BBA) Enzym.* **1980**, *615*, 158–166. [[CrossRef](#)]
25. Lu, D.; Fütterer, K.; Korolev, S.; Zheng, X.L.; Tan, K.; Waksman, G.; Sadler, J.E. Crystal structure of enteropeptidase light chain complexed with an analog of the trypsinogen activation peptide. *J. Mol. Biol.* **1999**, *292*, 361–373. [[CrossRef](#)] [[PubMed](#)]

26. Petrenko, D.E.; Nikolaeva, A.Y.; Lazarenko, V.A.; Dorovatovskii, P.V.; Timofeev, V.; Vlaskina, A.V.; Korzhenevskiy, D.A.; Mikhailova, A.G.; Rakitina, T.V. Screening of Conditions that Facilitate Crystallization of Oligopeptidase B from *Serratia Proteamaculans* by Differential Scanning Fluorimetry. *Crystallogr. Rep.* **2020**, *65*, 264–268. [[CrossRef](#)]
27. Petrenko, D.E.; Nikolaeva, A.Y.; Lazarenko, V.A.; Dorovatovskiy, P.V.; Timofeev, V.I.; Vlaskina, A.V.; Korzhenevskiy, D.A.; Mikhailova, A.G.; Boyko, K.M.; Rakitina, T.V. Crystallographic Study of Mutants and Complexes of Oligopeptidase B from *Serratia proteamaculans*. *Crystallogr. Rep.* **2020**, *65*, 909–914. [[CrossRef](#)]
28. Long, F.; Vagin, A.A.; Young, P.; Murshudov, G.N. BALBES: A molecular-replacement pipeline. *Acta Crystallogr. Sect. D Biol. Crystallogr.* **2007**, *64*, 125–132. [[CrossRef](#)] [[PubMed](#)]
29. Murshudov, G.N.; Skubák, P.; Lebedev, A.A.; Pannu, N.S.; Steiner, R.A.; Nicholls, R.A.; Winn, M.D.; Long, F.; Vagin, A.A. REFMAC5 for the refinement of macromolecular crystal structures. *Acta Crystallogr. Sect. D Biol. Crystallogr.* **2011**, *67*, 355–367. [[CrossRef](#)]
30. Emsley, P.; Lohkamp, B.; Scott, W.; Cowtan, K.D. Features and development of Coot. *Acta Crystallogr. Sect. D Biol. Crystallogr.* **2010**, *66*, 486–501. [[CrossRef](#)]
31. Krissinel, E.; Henrick, K. Inference of Macromolecular Assemblies from Crystalline State. *J. Mol. Biol.* **2007**, *372*, 774–797. [[CrossRef](#)] [[PubMed](#)]
32. Number 4 Collaborative Computational Project. The CCP4 suite: Programs for protein crystallography. *Acta Crystallogr. Sect. D Biol. Crystallogr.* **1994**, *50*, 760–763. [[CrossRef](#)] [[PubMed](#)]
33. Diederichs, K.; Karplus, P. Improved R-factors for diffraction data analysis in macromolecular crystallography. *Nat. Struct. Mol. Biol.* **1997**, *4*, 269–275. [[CrossRef](#)] [[PubMed](#)]
34. Holm, L. Using Dali for Protein Structure Comparison. *Methods Mol. Biol.* **2020**, *2112*, 29–42. [[CrossRef](#)]